A DFT study of molecular adsorption on titania-supported AuRh nanoalloys

Demiroglu, Ilker; Li, Ziyou; Piccolo, Laurent; Johnston, Roy L.

DOI:
10.1016/j.comptc.2017.02.012

Document Version
Publisher's PDF, also known as Version of record

Citation for published version (Harvard):
Demiroglu, I, Li, Z, Piccolo, L & Johnston, RL 2017, 'A DFT study of molecular adsorption on titania-supported AuRh nanoalloys', *Computational and Theoretical Chemistry*, vol. 1107, pp. 142–151. https://doi.org/10.1016/j.comptc.2017.02.012

Computational and Theoretical Chemistry 1107 (2017) 142–151

Contents lists available at ScienceDirect

Computational and Theoretical Chemistry

journal homepage: www.elsevier.com/locate/comptc

A DFT study of molecular adsorption on titania-supported AuRh nanoalloys

Ilker Demiroglu [a], Z.Y. Li [b], Laurent Piccolo [c], Roy L. Johnston [a,*]

[a] School of Chemistry, University of Birmingham, Edgbaston, Birmingham B15 2TT, United Kingdom
[b] Nanoscale Physics Research Laboratory, School of Physics and Astronomy, University of Birmingham, Edgbaston, Birmingham B15 2TT, United Kingdom
[c] Univ Lyon, Université Claude Bernard - Lyon 1, CNRS, IRCELYON - UMR 5256, 2 Avenue Albert Einstein, F-69626 VILLEURBANNE CEDEX, France

ARTICLE INFO

Article history:
Received 22 December 2016
Received in revised form 7 February 2017
Accepted 13 February 2017
Available online 17 February 2017

Keywords:
Au-Rh
Nanoalloys
Alloying effects
Support effects
d-band centre
Adsorption properties

ABSTRACT

$AuRh/TiO_2$ nanocatalysts have proved their efficiency in several catalytic reactions. In this work, density functional theory calculations are performed to investigate the effect of the TiO_2 support on the structures of fcc 38-atom and 79-atom AuRh nanoalloys and their adsorption properties towards the reactant molecules CO and O_2. d-band centre analysis shows that the d-band model captures the trends better for both larger and supported alloy clusters due to reduced mechanical effects. Calculations reveal metal-to-support electron transfer, depending mainly on which metal atoms lie at the interface with the support. The adsorption strengths of CO and O_2 molecules on experimentally-relevant Janus segregated structures are slightly lower than on pure Rh clusters, which may reduce poisoning effects, while maintaining the high reactivity of Rh. In addition, higher adsorption energies are predicted for the less stable $Au_{core}Rh_{shell}$ structure, which may lead to adsorption-induced restructuring under reaction conditions.

1. Introduction

Nanosized clusters have drawn the attention of many researchers due to their catalytic and other properties which are often different from their bulk counterparts. Nanoclusters are ideal catalysts since they possess a higher proportion of less-coordinated active sites in addition to their high surface/volume ratio. One well known example is ultra-fine gold nanoparticles, for which Haruta et al. [1] showed exceptional catalytic properties toward CO oxidation although gold is catalytically inert in the bulk phase [2].

Catalytic properties of metals can be improved by alloying different metals, due to synergistic effects, and nanoalloying allows catalytic properties to be tuned by varying composition and chemical ordering [3]. Furthermore, alloying an expensive but efficient catalyst (e.g. rhodium) with another, cheaper metal opens the possibility to reduce the cost of the catalyst without losing efficiency, or even sometimes improving it.

Among metal nanoalloys, the AuRh system has been scarcely studied [4–14] since the metals are immiscible in the bulk [15]. However, AuRh catalysts have been recently shown to be efficient in catalysing several reactions. For example, with respect to its monometallic counterparts, $AuRh/TiO_2$ showed increased catalytic stability in tetralin hydrogenation in the presence of H_2S [6], and improved selectivity for guaiacol hydrodeoxygenation [8].

The catalytic properties of multimetallic nanoalloys depend both on the chemical ordering and structures of the nanoparticles, which may vary with the molecular environment and the presence of a support. It is well known in the literature that the binding of ligands can change the chemical ordering and/or the structure of nanoparticles, thin films, and bulk surfaces [16–23]. For example, Tao et al. reported reversible core-shell inversion for Rh-Pd nanoparticles by controlling the molecular environment and suggested the design of "smart catalysts" that may catalyse different reactions depending on the gaseous environment [17,18]. Recently, our previous study of free Au-Rh nanoalloys also predicted, computationally, that the chemical ordering of Au-Rh nanoclusters can be changed due to CO or O_2 molecular environment [24]. Structure [25–27] and/or chemical ordering [7,28,29] of the nanoparticles also depends on the nature of the support. For the Au-Rh system, we have shown that the Janus-type phase-segregated nanoalloy structures become energetically competitive with the gas-phase core-shell structures when supported on TiO_2, and can be formed depending on the applied thermal post-treatment [6–8]. In practical heterogenous catalysis applications, nanoclusters are usually deposited or grown on supports. Understanding support effects on the catalyst structure and the cluster-adsorbate interaction is

* Corresponding author.
E-mail address: r.l.johnston@bham.ac.uk (R.L. Johnston).

http://dx.doi.org/10.1016/j.comptc.2017.02.012
2210-271X/

important, since the catalytic performance depends on both factors.

Adsorption of reactants is a key step in catalytic reactions, and can serve as a descriptor of the overall reactivity. According to Sabatier's principle, if reactive species are adsorbed too weakly, they may not be activated to undergo reaction, whereas if they are adsorbed too strongly, the desorption rate decreases and poisoning may occur. The d-band model [2,30] has been shown to be particularly useful in understanding metal-adsorbate interactions, especially for extended metal surfaces. In this model, the d-band energy centre of the metal surface or particle is used as a descriptor to predict the metal-adsorbate interaction strength.

In this work, we have studied the effect of the TiO_2 support on both the structures and reactivities of AuRh nanoalloys, focussing on the adsorption of CO and O_2 on AuRh clusters anchored on a rutile $TiO_2(1\,1\,0)$ surface, to model the titania nanorods used in experimental studies. In the following section, details are presented of our computational model. In the third section, the effect of the TiO_2 support on the chemical ordering of Au-Rh nanoalloys is presented. In the fourth and fifth sections, results are presented for CO and O_2 adsorption on AuRh/TiO_2, respectively, and a comparison is made to previous results obtained for free clusters. In the last section, adsorption properties are discussed within the framework of the d-band model.

2. Methodology

38-atom and 79-atom fcc-packed truncated octahedra (TO) were chosen as models for the bimetallic nanoparticles due to the high symmetry of the parent TO structure (O_h). Different compositions and alloying morphologies were covered by constructing several nanoalloy models within TO structures including mixed (ordered alloy), core-shell, Janus, and ball-cup [7] particles. For supported TO_{38} clusters, the surface-decorated "hex" structure (h-$Au_{32}Rh_6$) [20] is also considered for comparison purposes. Although 38- and 79- atom TO structures are smaller than the experimental particles (ca. 3 nm) [6–8], previous results showed that the mixing properties and energetics of Au-Rh nanoalloys scale well up to at least the 260-atom TO (~2 nm) [24], which is closer to the size range of the experimental particles.

The 38-atom Au, Rh and Au-Rh TO clusters are initially placed in three different orientations on the $TiO_2(1\,1\,0)$ surface, as shown in Fig. 1. For TO_{79} clusters, only position-1 was considered because it was found to maximise the cluster-surface interaction. Adsorption studies on both free and $TiO_2(1\,1\,1)$-supported nanoalloy clusters were carried out for CO and O_2 molecules. The adsorbates are placed on the $TiO_2(1\,1\,1)$-supported nanoalloy clusters according to the previous results obtained for free clusters, for all possible adsorption sites and coordination modes [24]. On supported clusters, adsorbates are placed both at positions close to and far from the cluster-substrate interface, in order to evaluate the effect of the substrate.

All density functional theory (DFT) calculations were performed with the Vienna ab initio Simulation Package (VASP) [31–34]. The generalized gradient approximation (GGA) Perdew-Burke-Ernzerhof (PBE) [35] exchange-correlation functional was adopted. The valance electron density was expanded in a plane wave basis set with a plane wave cut-off energy of 400 eV. The interaction between valence electrons and ionic cores was described by the projector augmented wave (PAW) method [36,37]. Methfessel-Paxton smearing, with a σ value of 0.01 eV, was implemented to improve convergence of metallic systems [38] Spin polarization was included in all DFT calculations. A sufficiently large unit cell was used to avoid interactions between periodic images of both free and supported metal clusters: resulting in a 3×6 TiO_2 supercell with lateral dimensions of a = 17.74 Å and b = 19.55 Å for both TO_{38} and TO_{79}. For supported cluster calculations, a nine-atomic layer TiO_2 slab was used to model the $TiO_2(1\,1\,0)$ substrate. The bottom three atomic layers of the slab were frozen during DFT optimizations to model bulk atoms. A vacuum spacing of over 10 Å vacuum was introduced for the supported cluster calculations to eliminate spurious cluster-surface interactions with the underneath of the surface slab. Only one k-point (at Γ) was used to sample the Brillouin zone due to the large size of the unit cell. Apart from the bottom three atomic layers of the TiO_2 slab, all other atom positions were optimized until all the forces on the atoms were lower than 0.01 eV/Å. Electronic ground states were determined after reaching a total energy convergence of 10^{-6} eV.

A mixing (or excess) energy term (Δ) was calculated to enable comparison of the energetics of nanoalloys with different compositions:

$$\Delta = E_{tot}(A_mB_n) - m\frac{E_{tot}(A_{m+n})}{m+n} - n\frac{E_{tot}(B_{m+n})}{m+n} \quad (1)$$

where the total energy (E_{tot}) of the nanoalloy A_mB_n is compared to the pure metal clusters of A and B of the same size ($m+n$). Hence, a negative value of Δ means an energy decrease upon mixing and therefore favourable mixing, whereas positive values indicate a demixing tendency. To determine the effect of the support and adsorbed molecules on nanoalloy energetics, Δ' was defined in the same manner as Δ by replacing the E_{tot} values with the total energy of the corresponding supported and/or molecule-adsorbed (nanoalloy and pure metal) clusters. The adsorption energy (E_{ads}) values

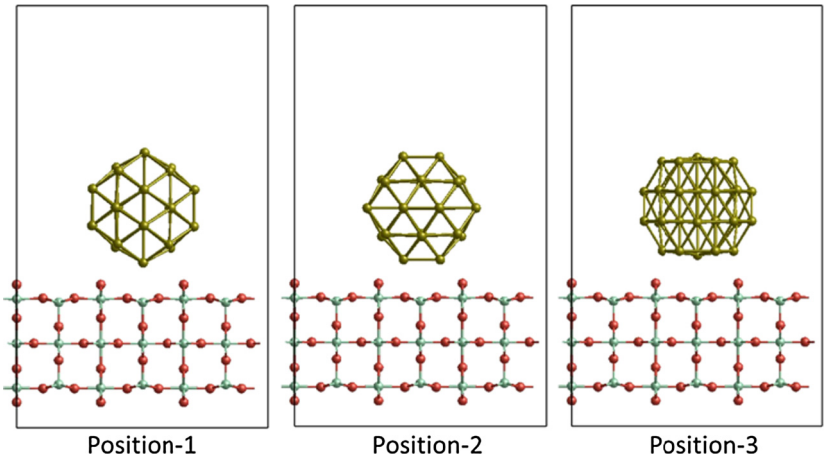

Fig. 1. Initial cluster-surface configurations for TO_{38} on $TiO_2(1\,1\,0)$. Example is given for a Au cluster.

were calculated as the differences in energy between the combined and separated systems.

3. Results

3.1. Supported Au-Rh cluster structure

Fig. 2 summarises the adsorption energies of the nanoalloy clusters for the three considered cluster binding positions (orientations). For TO_{38}, while the pure Au cluster prefers position–3 (E_{ads} = −5.88 eV), the pure Rh cluster prefers position-1 (E_{ads} = −8.98 eV). The cluster-surface binding strength is higher for Rh than for Au for all positions. The Au cluster shows distortion from its initial TO structure while the Rh cluster preserves its structure and adapts to the surface via rotation in positions 2 and 3. For the Janus cluster, the binding strength is very similar to that of the pure Rh cluster if it is bonded to the TiO_2 surface via the Rh, while position–1 is the preferred position as for pure Rh (E_{ads} = −8.93 eV) since this configuration maximises Rh-O interactions. However, if the Janus cluster is attached to the surface via Au, the binding strength decreases (by 2.54 eV for the best configuration) relative to the pure Au case, due to both electronic (less charge transfer than pure Au; see Table 1) and mechanical (Rh layers do not permit Au atoms to reconstruct sufficiently on the support) effects. Similarly, the binding strength for the $Rh_{core}Au_{shell}$ particle (−2.89 eV) is smaller than for the pure Au and Janus particles (−5.88 eV and −3.35 eV, respectively), since the core-shell structure restricts Au structural relaxation more than in the Janus particle although the extent of charge transfer is the same for the Janus structure.

Since the interaction with the TiO_2 surface is higher for Rh than Au, position–3 is the preferred position for the h-$Au_{32}Rh_6$ structure, where all the Rh atoms can interact with the TiO_2 surface. However, the binding strength is lower than for the pure Rh cluster due to the weaker Au-surface interaction energy.

The cluster-surface interaction energies for the $Au_{core}Rh_{shell}$ configuration are similar to those for the pure Rh cluster. Although it has almost the same value for position–1, it is increased for positions 2 and 3. For position–2, while pure Rh adapts to the support by rotation, the larger Au core expands the structure so that the Rh atoms on the bottom (1 0 0) facet are closer to the titania surface in the $Au_{core}Rh_{shell}$ configuration.

In principle, the total energy values give a direct comparison of stabilities of same composition clusters. However, as we cannot directly compare the total energies of different supported clusters with different compositions, such as Janus and $Rh_{core}Au_{shell}$, we have used a supported mixing energy term (Δ') to compare the stabilities, as shown in Fig. 3. Note that, by definition, the mixing energy differences of clusters with the same composition are equal to their total energy differences. When we compare the mixing energies of homotops with the same composition (supported h-$Au_{32}Rh_6$ and $Rh_{core}Au_{shell}$) the energy difference decreases to 3.0 eV for position–1 and position–2 and 1.7 eV for position–3, from the value of 5.28 eV for unsupported clusters, due to the excess adsorption energy. The energy difference is smallest for position–3, where the h-$Au_{32}Rh_6$ cluster benefits from all 6 Rh atoms being bonded to the TiO_2 support. According to Fig. 3, the $Rh_{core}Au_{shell}$ configuration is destabilised for all positions (more positive values than unsupported cluster), whereas h-$Au_{32}Rh_6$ maintains a similar stability for positions 1 and 2, but is stabilised in position-3. The Janus particle is stabilised relative to the other mixed clusters in all positions if it is bonded to the support via Rh atoms, while it is destabilised for all positions when bonded via Au atoms. For positions 1 and 3 the Δ' values also change sign and become negative for the Janus particle and for position–3 the energy difference with the $Rh_{core}Au_{shell}$ decreases to 0.12 eV from the value of 5.39 eV for the unsupported clusters. The $Au_{core}Rh_{shell}$ particle is also stabilised by bonding to the support, however the supported mixing energy value is still highly positive due to the unfavourable "inverse" core-shell configuration.

When we move to the larger TO_{79} clusters on the TiO_2 support, the binding properties remain similar. The detailed results for supported TO_{79} clusters have been reported elsewhere [24]. As for

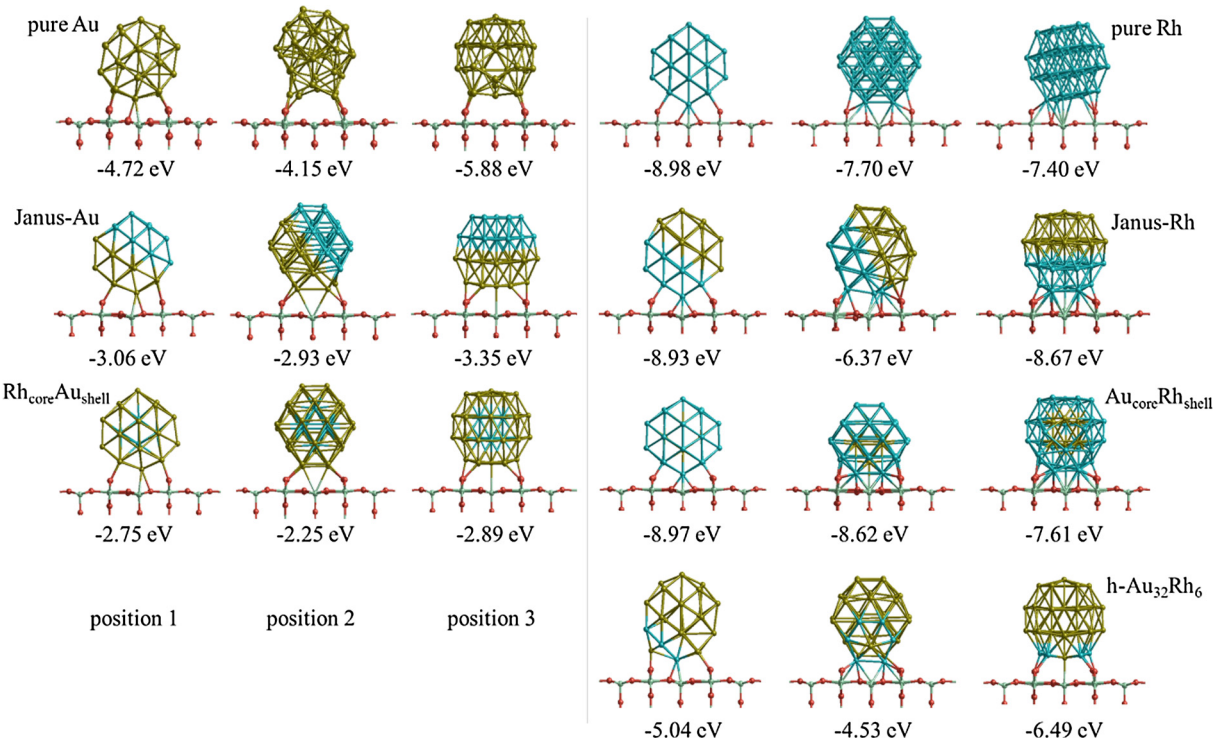

Fig. 2. Binding positions (orientations) and adsorption energies of Au, Rh, and Au-Rh TO_{38} nanoalloys on TiO_2(1 1 0) support. Blue, yellow, cyan and red spheres represent Rh, Au, Ti and O atoms, respectively. (For interpretation of the references to colour in this figure legend, the reader is referred to the web version of this article.)

Table 1
Total charges on Au atoms and on Rh atoms together with d-band centre values of all Au and all Rh atoms for all free and supported clusters. Charges on the TiO_2 support are also included for the TO_{38}/TiO_2 systems.

System	Charge (TiO_2)	Charge (Au)	Charge (Rh)	d-centre (Au)	d-centre (Rh)
TO_{38}					
Au	–	0.00	–	−3.42	–
$Rh_{core}Au_{shell}$	–	−1.35	1.35	−2.78	−1.32
Janus	–	−1.31	1.31	−2.87	−1.58
$Au_{core}Rh_{shell}$	–	−0.35	0.35	−4.16	−1.47
Rh	–	–	0.00	–	−1.73
TO_{38}/TiO_2					
Au	−2.22	2.22	–	−3.43	–
$Rh_{core}Au_{shell}$	−1.77	0.37	1.40	−2.95	−1.62
Janus-Au	−1.78	0.34	1.44	−3.09	−1.81
Janus-Rh	−2.50	−0.85	3.35	−3.00	−1.86
$Au_{core}Rh_{shell}$	−2.64	−0.70	3.34	−4.21	−1.66
Rh	−2.66	–	2.66	–	−1.87
TO_{79}					
Au	–	0.00	–	−2.94	–
$Rh_{core}Au_{shell}$	–	−3.19	3.19	−2.99	−1.55
$Rh_{ball}Au_{cup}$	–	−2.15	2.15	−3.01	−1.59
Janus	–	−1.68	1.68	−3.03	−1.56
$Au_{core}Rh_{shell}$	–	−1.03	1.03	−3.88	−1.39
Rh	–	–	0.00	–	−1.83
TO_{79}/TiO_2					
Au	−1.90	1.90	–	−3.10	–
$Rh_{core}Au_{shell}$	−1.97	−1.26	3.23	−3.11	−1.73
$Rh_{ball}Au_{cup}$-Au	−1.97	−0.13	2.10	−3.14	−1.79
Janus-Au	−1.96	0.13	1.83	−3.15	−1.75
Janus-Rh	−3.20	−1.83	5.03	−3.15	−1.84
$Rh_{ball}Au_{cup}$-Rh	−3.07	−1.22	4.29	−3.14	−1.80
$Au_{core}Rh_{shell}$	−3.14	−1.57	4.71	−3.98	−1.56
Rh	−3.31	–	3.31	–	−1.94

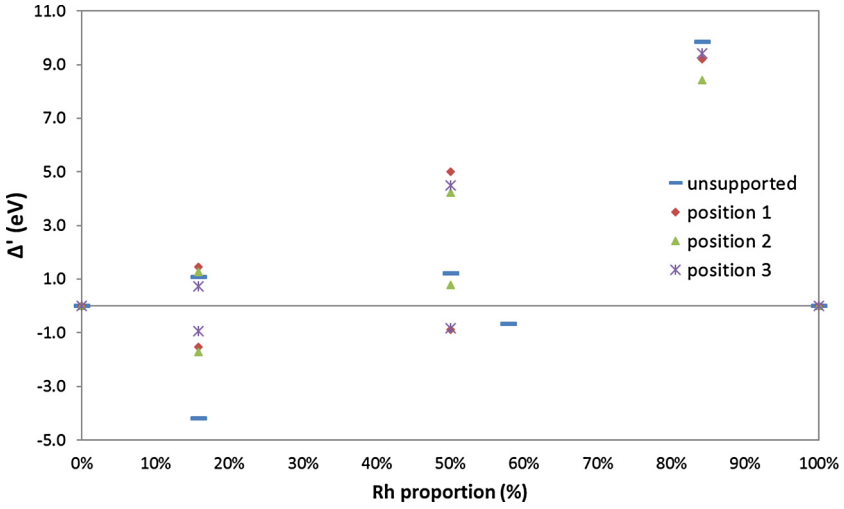

Fig. 3. Supported mixing energy (Δ′) values versus Rh proportion for TO_{38}/TiO_2 at three binding positions, compared to unsupported TO_{38}.

TO_{38}, the metal-support binding is found to be stronger for Rh than for Au in the case of TO_{79}.

In summary, the binding strength for nanoalloy clusters is governed by the type of atoms in contact with the TiO_2 surface. The Janus and ball-cup clusters, whose Rh atoms bind to the TiO_2 surface, become more stable on the support, whereas the initially stable $Rh_{core}Au_{shell}$ cluster is destabilised.

3.1.1. Electronic analysis

Bader charge analysis [39] reveals Rh-to-Au electron transfer for free alloy clusters, as expected since Rh is more electropositive than Au (see Table 1). For $Rh_{core}Au_{shell}$ and Janus clusters the transferred charge is almost the same (∼ 1.3 e) in the case of small clusters (TO_{38}), while for larger clusters (TO_{79}) the charge transfer increases as the core proportion of Rh increases. Charge transfer is significantly lower from shell Rh to core Au in the $Au_{core}Rh_{shell}$ clusters, which is consistent with the fact that in homometallic Rh clusters the surface sites actually tend to be negatively charged relative to the core. When supported, we observe metal to support charge transfer for both pure and alloy clusters. The metal-to-support charge transfer is generally greater for larger particles, with the exception of Au_{38}. This is probably because the TO structure of Au_{38} is highly reconstructed on TiO_2, while for alloy clusters the presence of the Rh atoms reduces Au atom relaxation. Metal to

support charge transfer is also found to be greater when Rh is in contact with the TiO_2 support.

DOS analysis shows an upward shift of the Rh d-band centre for alloy clusters for both sizes (see Table 1). For TO_{38}, the Rh d-band centre shift is highest for $Rh_{core}Au_{shell}$ and lowest for the Janus particle, both for supported and free clusters. However, for the larger TO_{79}, clusters the Rh d-centre shift is greatest for $Au_{core}Rh_{shell}$, while $Rh_{core}Au_{shell}$ and Janus particles behave similarly. The Au d-band centre shows a slight downward shift upon alloying, with the exception of $Rh_{core}Au_{shell}$ and Janus particles for smaller TO_{38}. For $Rh_{core}Au_{shell}$ and Janus configurations of TO_{38}, the d-band centre shifts upwards significantly relative to pure Au. On the TiO_2 support, all the d-band centres showed a downward shift by 0.01–0.20 eV compared to the unsupported counterparts. However, this shift is not just due to the lower occupation of the d-band since the d-band centres are integrated over all d-states, including unoccupied ones.

3.2. Molecular adsorption on supported Au-Rh nanoalloys

Position-1 binding of the clusters has been chosen for the molecular adsorption studies because it maximises the nanocluster-support interaction, especially for the more favourable Rh-support-contact case. CO and O_2 molecules are placed systematically on convenient sites according to their adsorption properties on free Au-Rh nanoalloys [24]. For both TO_{38} and TO_{79}, CO molecules were initially placed at bridge positions on the edges of the metal particles in a $\mu_2\eta^1$ type binding fashion, one being close to the support and the other far from it. Here the symbol μ stands for the number of metal atoms to which the adsorbate binds and the symbol η stands for the number of atoms in the adsorbate which are bonded to the metal. O_2 molecules are also placed on edges of metal particles though with $\mu_2\eta^2$ type binding since both O atoms tend to bind metal atoms. For O_2 molecules interfacial sites, where the O_2 molecule bridges a cluster metal atom and a surface Ti atom, were also included.

3.2.1. CO adsorption on supported TO_{38}

Fig. 4 shows the structures and adsorption energies of CO molecules adsorbed on $\mu_2\eta^1$ bridge sites on TiO_2-supported TO_{38} nanoalloy clusters, both for positions close to and far from the cluster-support interface. As for the unsupported clusters [24], the CO adsorption energies for the supported alloy clusters are significantly higher when the CO molecule is adsorbed on Rh atoms than on Au atoms. For supported Au_{38}, the CO adsorption strength decreases by ~0.5 eV on the TiO_2 support relative to the unsupported cluster for both adsorption sites considered. CO adsorption close to the support is 0.14 eV more stable than far from the support. On the contrary, for pure Rh, CO adsorbed far from the support is 0.05 eV more stable than close to the support. For supported Rh_{38}, the CO adsorption strengths are increased by 0.03 eV and 0.05 eV for adsorption sites far from and close to the support, respectively, relative to their unsupported counterparts.

For $Rh_{core}Au_{shell}$, which is the most stable isomer for the free Rh-Au clusters, the CO adsorption strength increases relative to the unsupported case by 0.16 eV for CO close to the support and 0.19 eV for CO adsorbed far from the support. It has been shown that for free clusters, the CO adsorption strength decreases for $Rh_{core}Au_{shell}$ relative to the pure Au cluster.[24] However, with the inclusion of the support, the adsorption strengths become similar due to the reverse effect of the TiO_2 support on pure Au and $Rh_{core}Au_{shell}$ clusters. In contrast, for the $Au_{core}Rh_{shell}$ cluster, which is the least stable isomer in free space, the CO adsorption energies for close to the support and far from the support show opposite trends as compared to adsorption on free clusters. The adsorption strength increases slightly (by 0.02 eV) for the position far from the support, as in pure Rh_{38}, while it decreases for the position close to the support by 0.20 eV, contrary to pure Rh_{38}.

For the Janus particle attached to the support through Au (Janus-Au), which is relatively unstable, the CO adsorption strength on the Au side increases by 0.16 eV relative to the free cluster, similar to the $Rh_{core}Au_{shell}$ case. When the CO molecule is adsorbed on the Rh side, however, the adsorption strengths decrease for sites both far and close to the support, unlike for the pure Rh case. For the Janus particle attached to the support through Rh side (Janus-Rh), which is stabilised due to the support, the CO adsorption strength on the Au side decreases when it is far from the support (similar to pure Au_{38}) while it increases slightly for CO adsorbed close to the support (similar to $Rh_{core}Au_{shell}$). When the CO molecule is adsorbed on the Rh side, the adsorption strength decreases by 0.20 eV relative to the unsupported cluster, unlike for pure Rh_{38}.

3.2.2. CO adsorption on supported TO_{79}

For larger particles, the effect of the support on CO adsorption is found to be more straight-forward than for TO_{38} because mechanical effects such as strain and relaxation are reduced. Fig. 5 shows the structures and adsorption energies of CO molecules adsorbed on TiO_2-supported TO_{79} nanoalloy clusters both for sites close to and far from the cluster-support interface. For $Rh_{core}Au_{shell}$ and $Rh_{ball}Au_{cup}$, in which the core Rh atoms make the cluster structure more rigid, the CO adsorption strength on the Au side is almost

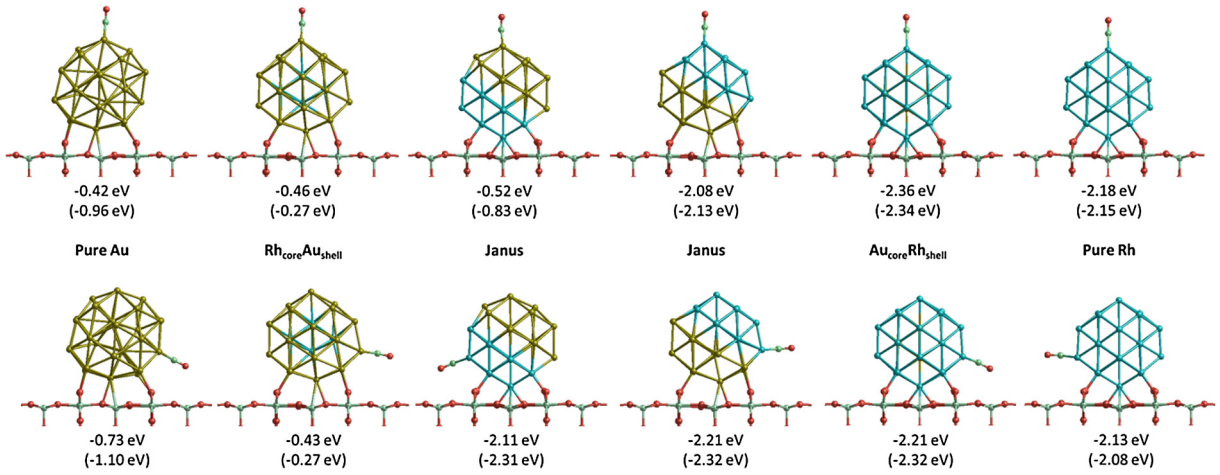

Fig. 4. Structures and CO adsorption energies of TiO_2-supported TO_{38} clusters. Numbers in parentheses are the CO adsorption energies of the corresponding unsupported clusters.

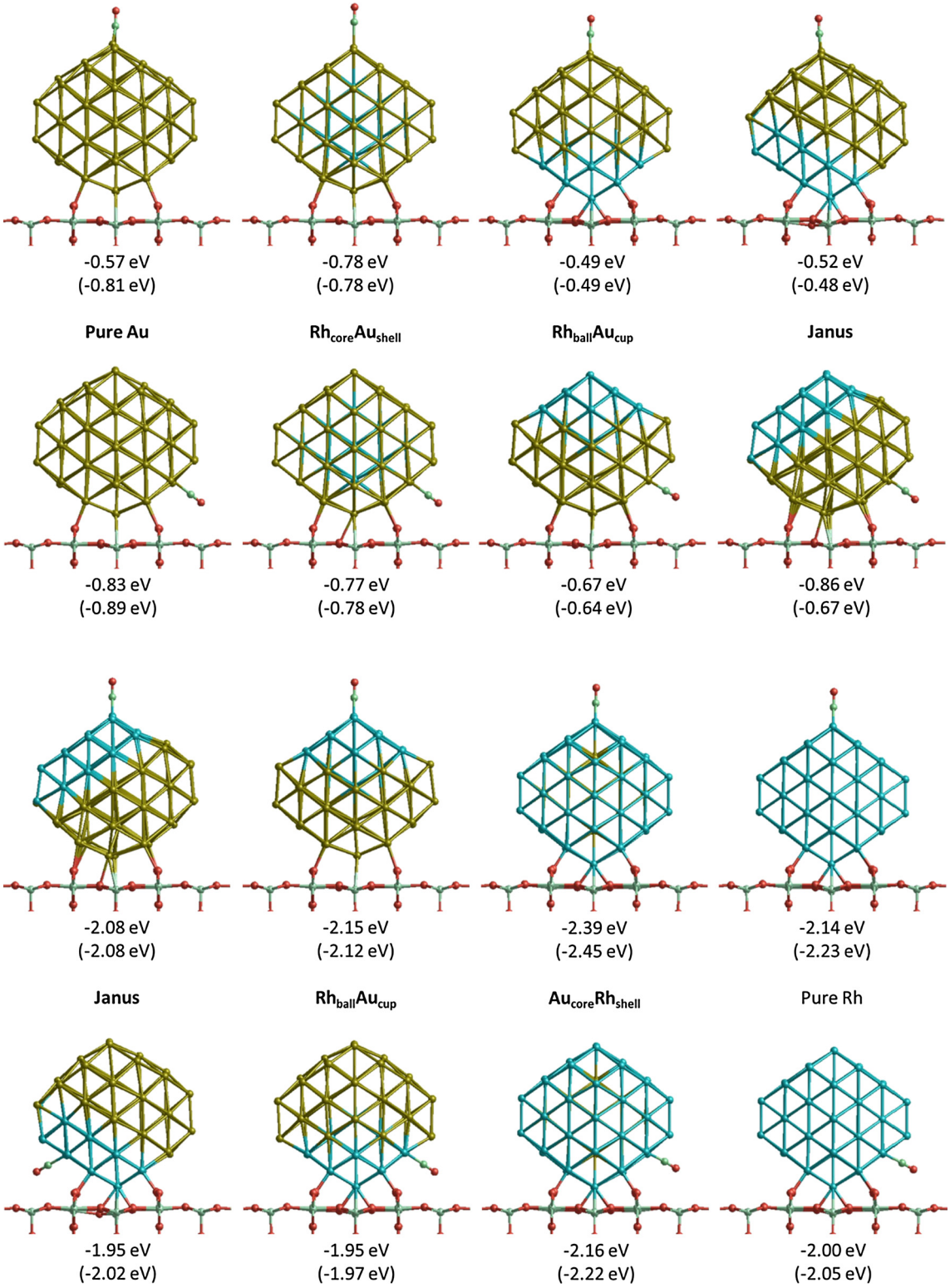

Fig. 5. Structures and CO adsorption energies of TiO_2-supported TO_{79} clusters. Numbers in parentheses are the adsorption energies on the corresponding unsupported clusters.

unchanged. The maximum change (0.03 eV) with respect to free clusters is found for $Rh_{ball}Au_{cup}$ when it interacts with the support via Au atoms, which allows larger distortions at the interface. Similarly, on the Janus particle, the adsorption strength significantly increases (by 0.19 eV) when the Au layers are at the interface with the TiO_2 support. For pure gold, the adsorption strength is reduced on supported clusters, and "close" adsorption sites are preferred over "far" ones. The change in the adsorption strength is greater for far positions, where there is more structural distortion of the Au particle. The strongest adsorption for CO molecules on Au atoms is found for the Janus-Au case, which is relatively unstable, both for supported and free clusters. When we compare the stable supported clusters, CO adsorption is weaker on the Au sides of alloy clusters than on pure Au.

CO adsorption on the Rh sides of nanoalloys is much stronger than on the Au sides, as expected. Due to the effect of the support, the CO adsorption strength is reduced (by ~0.05 eV), except for Janus and $Rh_{ball}Au_{cup}$ clusters when they are linked to the support via Au atoms. The adsorption strength is a maximum for the Au_{core}-Rh_{shell} cluster, which is the least stable configuration both for free and supported clusters. For the Janus and $Rh_{ball}Au_{cup}$ clusters, which are stable on TiO_2 via Rh contact, the CO adsorption strengths are found to be the same (1.95 eV) and slightly lower (0.05 eV) than for pure Rh_{79}, respectively.

3.2.3. O_2 adsorption on TO_{38}

Fig. 6 shows the structures and adsorption energies of O_2 molecules adsorbed on $\mu_2\eta^2$ bridge sites on TiO_2-supported TO_{38} nanoalloy clusters for close, far and interfacial positions. On pure Au, the adsorption strength of O_2 drops significantly compared to free clusters. However, on $Rh_{core}Au_{shell}$ the O_2 adsorption strength is still lower than on pure Au_{38}, although it is increased slightly (by 0.05 eV) relative to the unsupported cluster when close to the support. O_2 adsorption on Au side of the Janus cluster is stronger than on pure Au_{38}, unlike for free clusters. For Janus particles, the O_2 adsorption strength on the Au side increases when the metal cluster has Rh in contact with the support, while it decreases for Au contact, as for CO adsorption.

On the Rh side of supported 38-atom alloy clusters, O_2 adsorption strength increases relative to the unsupported counterparts, except for the Janus particle when it is attached to the support through Au side. For this Janus configuration, the adsorption strength is 0.12 eV lower than for pure Rh, although it was 0.13 eV higher for free clusters. However, when the Janus particle is attached to the support via Rh atoms, the O_2 molecule spontaneously dissociates on neighbouring Rh atoms. For the unstable $Au_{core}Rh_{shell}$ the adsorption is found stronger than pure Rh.

When O_2 molecule is adsorbed on interfacial sites of 38-atom metal clusters supported on titania, the adsorption strength increases significantly when Au sides of the particles are involved, with the pure Au one having the highest adsorption strength. However, although being approximately 1 eV stronger than on Au sides, peripheral positions on Rh sides of metal clusters are less favourable than O_2 molecules binding to two neighbouring Rh atoms. For the peripheral adsorption position, highest adsorption strength (adsorption energy = −2.22 eV) is found for the Janus particle.

3.2.4. O_2 adsorption on supported TO_{79}

When particle size increases, the effect of the support is lower for O_2 adsorption on 79-atom nanoalloy clusters (see Fig. 7). Only pure Au and $Rh_{core}Au_{shell}$ structures show more than 0.05 eV differences from free clusters. Adsorption energies on Au sides are very small (between −0.10 eV and −0.25 eV) when the O_2 molecule is bonded to two neighbouring Au atoms, while $Rh_{core}Au_{shell}$ has the highest adsorption strength. Adsorption strength increases when O_2 binds one Au atom and one surface Ti atom. For this configuration, pure Au and $Rh_{core}Au_{shell}$ lead to the strongest and weakest adsorption, respectively. The Janus and $Rh_{ball}Au_{cup}$ structures behave similarly in adsorption of O_2 on both their Au and Rh sides. For $Rh_{ball}Au_{cup}$, since the considered adsorption site close to the support does not allow both O atoms to bond to adjacent Rh atoms on the cluster surface, one O atom binds to an Au atom. Thus, the adsorption energy (−1.09 eV) is lower than on Rh, while it is similar to that of an O_2 molecule bridging a Ti atom and an Au atom (−1.10 to −1.34 eV). For larger particles (TO_{79}), the O_2 adsorption strength is maximal for $Au_{core}Rh_{shell}$ clusters, both for free and supported clusters, as in the CO case. Similarly, O_2 adsorption is weaker on phase-segregated Janus and $Rh_{ball}Au_{cup}$ structures for free and supported clusters.

3.2.5. d-band centre analysis

Surface d-bands of metal alloys are affected by both ligand [40,41] and strain [42,43] effects. It is difficult to separate these two effects for extended surfaces [44], but it is possible for finite clusters [24]. However for the latter, one should be careful since low-coordinated sites [45] complicate the picture relative to extended surfaces, in addition to more prominent relaxation [46,47] and reconstruction [21,48,49] effects, which may be induced by adsorbates.

According to the d-band model [30], an upshift in the d-band centre should correlate with higher adsorption strength. However, our previous results on molecular adsorption on free 38-atom AuRh clusters showed strong deviations from the d-band model, mainly because of mechanical effects such as strain and relaxation effects [24]. Higher deviations are observed for the adsorption of

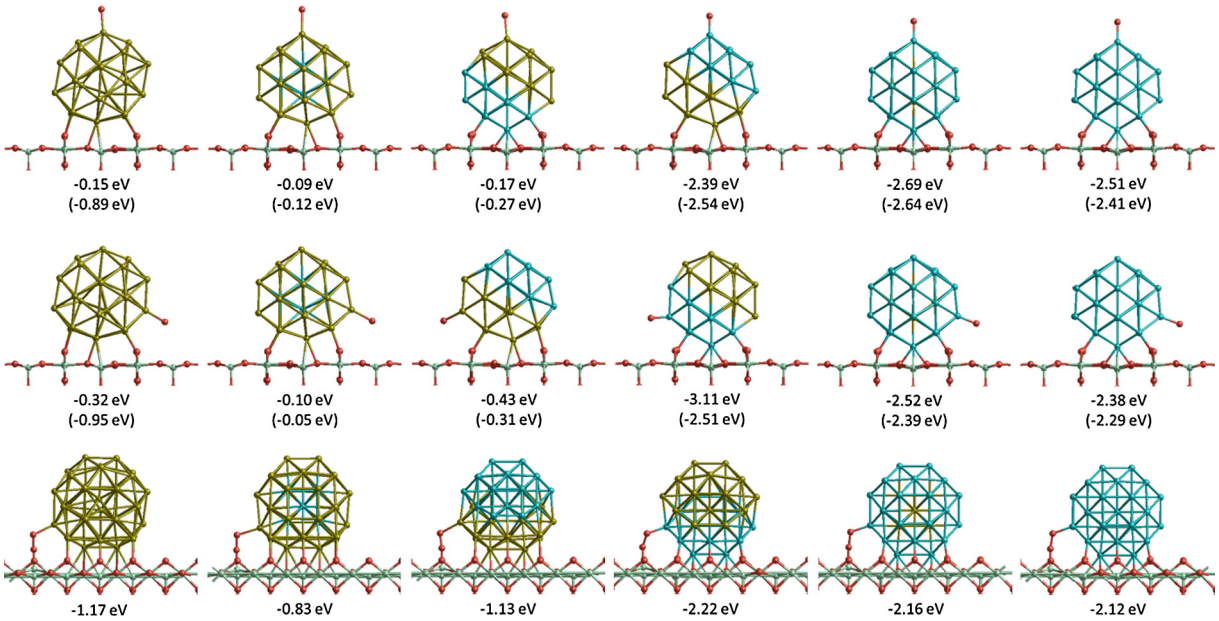

Fig. 6. Structures and O_2 adsorption energies of TiO_2-supported TO_{38} clusters. Numbers in parentheses are the adsorption energies on corresponding unsupported clusters.

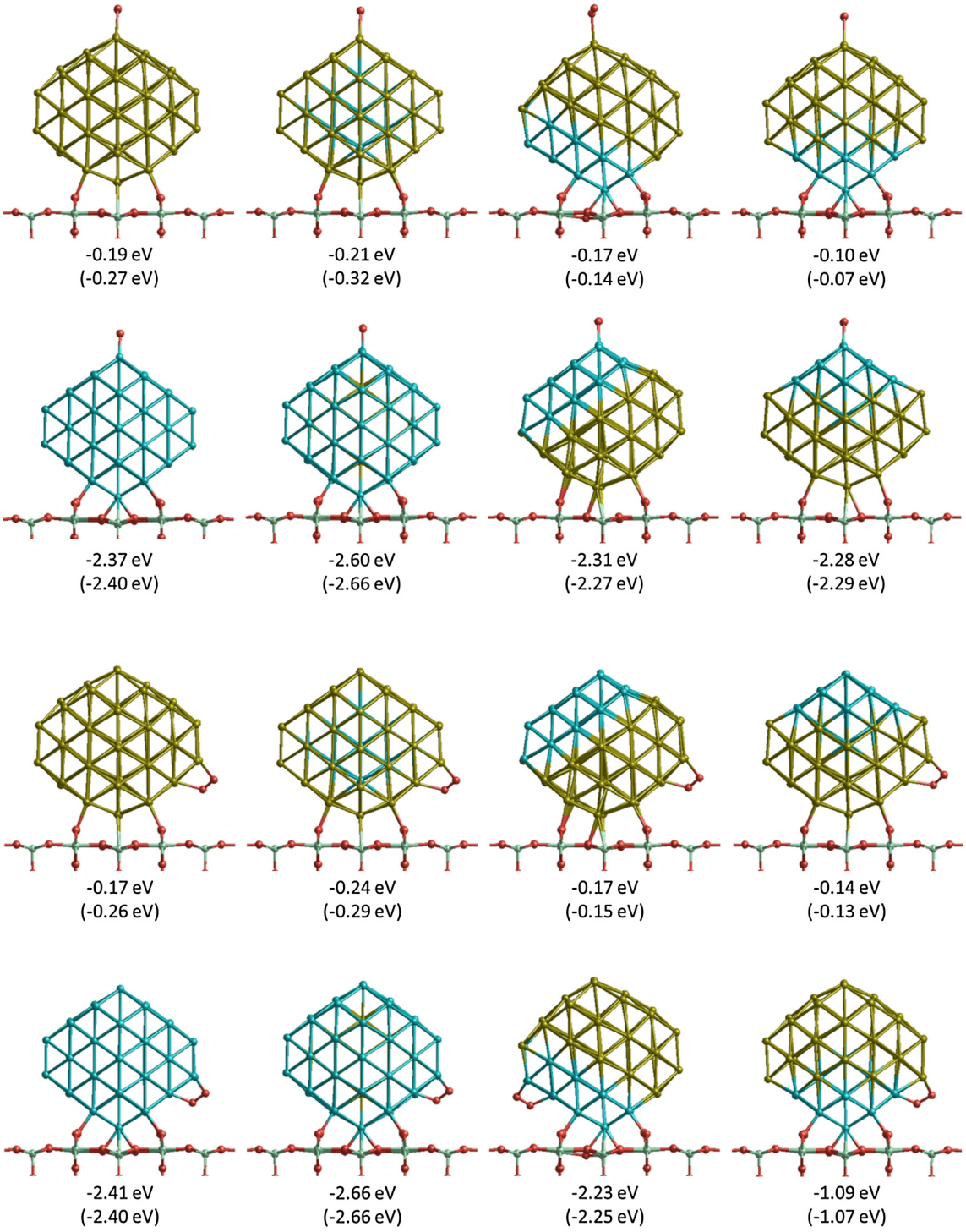

Fig. 7. Structures and O_2 adsorption energies of TiO_2-supported TO_{79} clusters. Numbers in parentheses are the adsorption energies on the corresponding unsupported clusters.

CO and O_2 on the Au side of clusters, because of the greater structural flexibility of Au atoms than Rh atoms, which enhances mechanical effects. In addition, there is a repulsive contribution between the valence electrons of the adsorbates and the filled Au d-band [50], which is increased due to Rh to Au charge transfer.

Fig. 8 shows plots of adsorption energies versus d-band centres on free and supported TO_{38} and TO_{79} clusters. For TO_{38} clusters, the deviations are larger for free clusters (R^2 values are 0.78 for CO and 0.79 for O_2) than on the support (R^2 values are 0.91 for CO and 0.93 for O_2). This is possibly because alloying-induced cluster strain effects are generally reduced when the clusters are pinned on the support. For example, the average Au-Au distance increases for TO_{38} clusters on the support by 0.03–0.05 Å when they bound to the support through Au atoms. Mechanical effects are also reduced on increasing the cluster size so that the d-band model is more relevant for the larger TO_{79} clusters. When we compare the free and supported clusters, there is a 0.10 eV downward shift on average of the d-band centre values. Thus, the adsorption strength of CO and O_2 molecules on supported clusters is generally slightly reduced compared to their free counterparts.

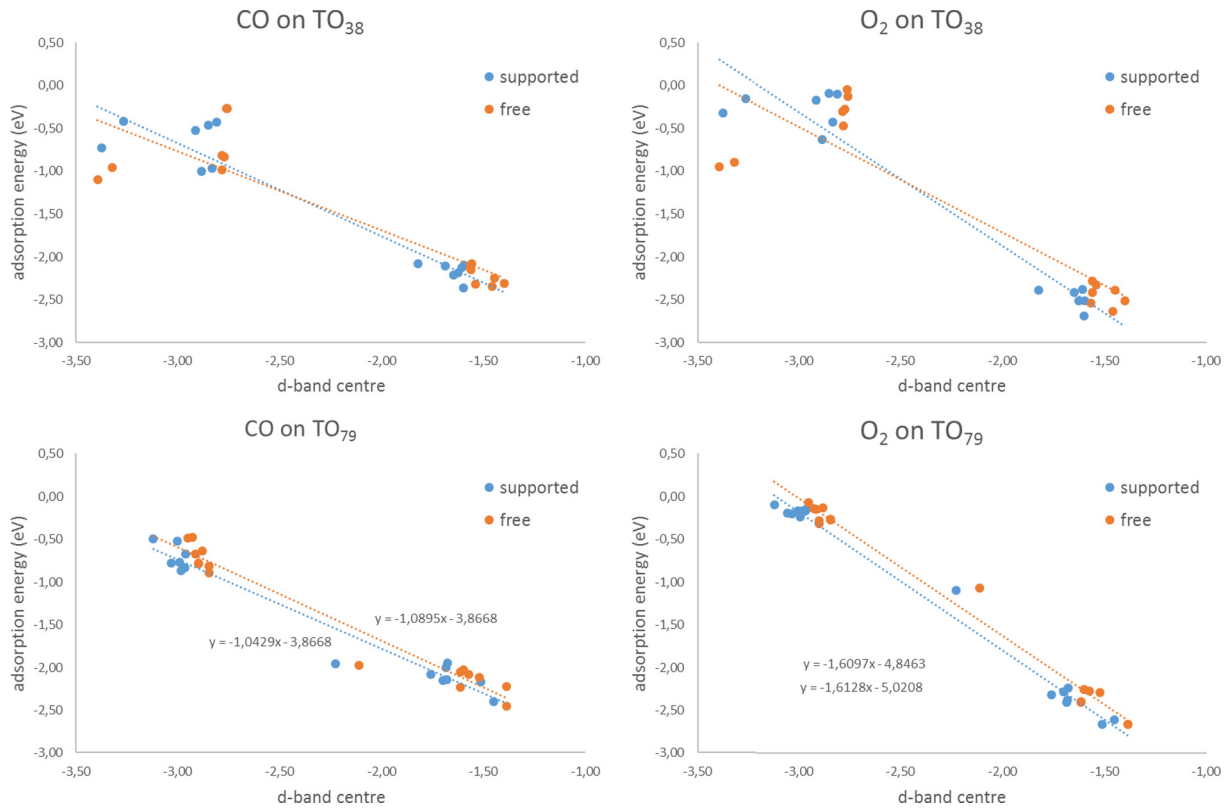

Fig. 8. Adsorption energy versus d-band centre for CO and O_2 adsorption on TO_{38} and TO_{79} clusters. Orange dots correspond to TiO_2-supported clusters while blue dots correspond to free clusters. Linear fits and corresponding R^2 values are given on each graph. (For interpretation of the references to colour in this figure legend, the reader is referred to the web version of this article.)

4. Conclusions

The effect of the TiO_2 support on both the structures of AuRh nanoalloys and their adsorption properties towards CO and O_2 have been investigated using first-principles DFT calculations. In agreement with experiments, on the TiO_2 support phase-segregated Janus-type structures are found to compete with the more stable free $Rh_{core}Au_{shell}$ structures. Bader charge analysis shows that there is metal-to-support electron transfer, which is higher when the more electropositive Rh atoms are located at the interface with the titania support. As for the free clusters, the adsorption strengths of reactant molecules such as O_2 and CO are greater on the Rh part than on the Au part of the supported nanoalloy clusters. The adsorption properties of smaller clusters are more diverse for free clusters because the mechanical effects reduce with the increasing size. With the presence of the support, however, mechanical effects also decrease for small clusters and it reduces the scattering in the d-band model. A downward shift of the d-band, which is accompanied by a slight reduction in CO and O_2 adsorption strengths, is observed for the supported AuRh nanoalloys compared to their free cluster counterparts.

Concerning the experimentally more relevant Janus-type structures, having Rh atoms at the interface with the TiO_2 surface, adsorption strengths on the Rh side of the cluster were found to be slightly lower than for pure Rh clusters. This may modify the catalytic properties, e.g. reduce poisoning, while still preserving the high reactivity of pure Rh as compared to both pure Au and $Rh_{core}Au_{shell}$ clusters. Furthermore, in contrast to the Janus particles, adsorption on the less stable $Au_{core}Rh_{shell}$ clusters is stronger than on pure Rh. Although the $Au_{core}Rh_{shell}$ structure is highly unstable for free clusters, its relative instability is reduced in the presence of the support, and it may be stabilised further by tuning the molecular environment [24].

Acknowledgments

This research was funded by the Engineering and Physical Sciences Research Council, UK (EPSRC) under Critical Mass Grant EP/J010804/1 "TOUCAN: Towards an Understanding of Catalysis on Nanoalloys". Calculations were performed on the following HPC facilities: The University of Birmingham BlueBEAR facility (see http://www.bear.bham.ac.uk/bluebear for more details) and the UK's national HPC facility, ARCHER, both via membership of the UK's HPC Materials Chemistry Consortium, which is funded by EPSRC (EP/L000202), and via the TOUCAN grant.

References

[1] M. Haruta, T. Kobayashi, H. Sano, N. Yamada, Novel gold catalysts for the oxidation of carbon monoxide at a temperature far below 0 °C, Chem. Lett. 16 (1987) 405–408, http://dx.doi.org/10.1246/cl.1987.405.
[2] B. Hammer, J.K. Norskov, Why gold is the noblest of all the metals, Nature 376 (1995) 238–240, http://dx.doi.org/10.1038/376238a0.
[3] R. Ferrando, J. Jellinek, R.L. Johnston, Nanoalloys: From theory to applications of alloy clusters and nanoparticles, Chem. Rev. 108 (2008) 845–910, http://dx.doi.org/10.1021/cr040090g.
[4] R.L. Chantry, I. Atanasov, S.L. Horswell, Z.Y. Li, R.L. Johnston, Interfacial structures and bonding in metal-coated gold nanorods, Struct. Bond. (2014) 67–90, http://dx.doi.org/10.1007/430_2013_139.
[5] S. García, L. Zhang, G.W. Piburn, G. Henkelman, S.M. Humphrey, Microwave synthesis of classically immiscible rhodium-silver and rhodium-gold alloy nanoparticles: Highly active hydrogenation catalysts, ACS Nano 8 (2014) 11512–11521, http://dx.doi.org/10.1021/nn504746u.
[6] Z. Konuspayeva, P. Afanasiev, T.-S. Nguyen, L. Di Felice, F. Morfin, N.-T. Nguyen, J. Nelayah, C. Ricolleau, Z.Y. Li, J. Yuan, G.D. Berhault, L. Piccolo, Au-Rh and Au-Pd nanocatalysts supported on rutile titania nanorods: structure and chemical stability, Phys. Chem. Chem. Phys. 17 (2015) 28112–28120, http://dx.doi.org/10.1039/C5CP00249D.
[7] L. Piccolo, Z.Y. Li, I. Demiroglu, F. Moyon, Z. Konuspayeva, G. Berhault, P. Afanasiev, W. Lefebvre, J. Yuan, R.L. Johnston, Understanding and controlling the structure and segregation behaviour of AuRh nanocatalysts, Sci. Rep. 6 (2016) 35226, http://dx.doi.org/10.1038/srep35226.

[8] T.S. Nguyen, D. Laurenti, P. Afanasiev, Z. Konuspayeva, L. Piccolo, Titania-supported gold-based nanoparticles efficiently catalyze the hydrodeoxygenation of guaiacol 344 (2016) 136–140, http://dx.doi.org/10.1016/j.jcat.2016.09.016.
[9] R.L. Chantry, W. Siriwatcharapiboon, S.L. Horswell, A.J. Logsdail, R.L. Johnston, Z.Y. Li, Overgrowth of rhodium on gold nanorods, J. Phys. Chem. C 116 (2012) 10312–10317, http://dx.doi.org/10.1021/jp212432g.
[10] R.L. Chantry, I. Atanasov, W. Siriwatcharapiboon, B.P. Khanal, E.R. Zubarev, S.L. Horswell, R.L. Johnston, Z.Y. Li, An atomistic view of the interfacial structures of AuRh and AuPd nanorods, Nanoscale 5 (2013) 7452–7457, http://dx.doi.org/10.1039/c3nr02560h.
[11] A. Berkó, R. Gubó, L. Óvári, Z. Kónya, Rh and Au deposited on ultrathin TiO $\sim$ 1.2 film formed on Rh(111) facets and the effects of CO exposure, Surf. Sci. 641 (2015) 300–304, http://dx.doi.org/10.1016/j.susc.2015.02.016.
[12] L. Óvári, A. Berkó, R. Gubó, Á. Rácz, Z. Kónya, Effect of a gold cover layer on the encapsulation of rhodium by titanium oxides on titanium dioxide(110), J. Phys. Chem. C 118 (2014) 12340–12352, http://dx.doi.org/10.1021/jp502748a.
[13] E.R. Essinger-Hileman, D. DeCicco, J.F. Bondi, R.E. Schaak, Aqueous room-temperature synthesis of Au–Rh, Au–Pt, Pt–Rh, and Pd–Rh alloy nanoparticles: fully tunable compositions within the miscibility gaps, J. Mater. Chem. 21 (2011) 11599, http://dx.doi.org/10.1039/c0jm03913f.
[14] S. García, R.M. Anderson, H. Celio, N. Dahal, A. Dolocan, J. Zhou, S.M. Humphrey, Microwave synthesis of Au-Rh core-shell nanoparticles and implications of the shell thickness in hydrogenation catalysis, Chem. Commun. 49 (2013) 4241–4243, http://dx.doi.org/10.1039/c3cc40387d.
[15] R.H. Davies, A.T. Dinsdale, J.A. Gisby, J.A.J. Robinson, S.M. Martin, MTDATA – Thermodynamic and phase equilibrium software from the national physical laboratory, CALPHAD: Comput. Coupling Phase Diagrams Thermochem. 26 (2002) 229–271, http://dx.doi.org/10.1016/S0364-5916(02)00036-6.
[16] K.J. Andersson, F. Calle-Vallejo, J. Rossmeisl, I. Chorkendorff, Adsorption-driven surface segregation of the less reactive alloy component, J. Am. Chem. Soc. 131 (2009) 2404–2407, http://dx.doi.org/10.1021/ja8089087.
[17] F. Tao, M.E. Grass, Y. Zhang, D.R. Butcher, F. Aksoy, S. Aloni, V. Altoe, S. Alayoglu, J.R. Renzas, C.K. Tsung, Z. Zhu, Z. Liu, M. Salmeron, G.A. Somorjai, Evolution of structure and chemistry of bimetallic nanoparticle catalysts under reaction conditions, J. Am. Chem. Soc. 132 (2010) 8697–8703, http://dx.doi.org/10.1021/ja101502t.
[18] F. Tao, M.E.E. Grass, Y. Zhang, D.R.R. Butcher, J.R.R. Renzas, Z. Liu, J.Y.Y. Chung, B.S.S. Mun, M. Salmeron, G.A.A. Somorjai, Reaction-driven restructuring of Rh-Pd and Pt-Pd core-shell nanoparticles, Science (80-). 322 (2008) 932–934, http://dx.doi.org/10.1126/science.1164170.
[19] P.S. West, R.L. Johnston, G. Barcaro, A. Fortunelli, Effect of CO and H adsorption on the compositional structure of binary nanoalloys via DFT modeling, Eur. Phys. J. D 67 (2013) 165, http://dx.doi.org/10.1140/epjd/e2013-40257-4.
[20] P.S. West, R.L. Johnston, G. Barcaro, A. Fortunelli, The effect of CO and H chemisorption on the chemical ordering of bimetallic clusters, J. Phys. Chem. C 114 (2010) 19678–19686, http://dx.doi.org/10.1021/jp108387x.
[21] L.O. Paz-Borbon, R.L. Johnston, G. Barcaro, A. Fortunelli, Chemisorption of CO and H on Pd, Pt and Au nanoclusters: A DFT approach, Eur. Phys. J. D 52 (2009) 131–134, http://dx.doi.org/10.1140/epjd/e2009-00041-9.
[22] J. Knudsen, A.U. Nilekar, R.T. Vang, J. Schnadt, E.L. Kunkes, J.A. Dumesic, M. Mavrikakis, F. Besenbacher, A Cu/Pt near-surface alloy for water-gas shift catalysis, J. Am. Chem. Soc. 129 (2007) 6485–6490, http://dx.doi.org/10.1021/ja0700855.
[23] O.M. Løvvik, S.M. Opalka, Reversed surface segregation in palladium-silver alloys due to hydrogen adsorption, Surf. Sci. 602 (2008) 2840–2844, http://dx.doi.org/10.1016/j.susc.2008.07.016.
[24] I. Demiroglu, Z. Li, L. Piccolo, R.L. Johnston, A DFT study of molecular adsorption on Au-Rh Nanoalloys, Catal. Sci. Technol. 6 (2016) 6916–6931, http://dx.doi.org/10.1039/C6CY01107A.
[25] G. Barcaro, A. Fortunelli, G. Rossi, F. Nita, R. Ferrando, Epitaxy, truncations, and overhangs in palladium nanoclusters adsorbed on MgO(001), Phys. Rev. Lett. 98 (2007) 156101, http://dx.doi.org/10.1103/PhysRevLett. 98.156101.
[26] L.B. Vilhelmsen, B. Hammer, Systematic study of Au 6 to Au 12 gold clusters on MgO(100) F centers using density-functional theory, Phys. Rev. Lett. 108 (2012) 126101, http://dx.doi.org/10.1103/PhysRevLett. 108.126101.
[27] R. Ferrando, G. Rossi, F. Nita, G. Barcaro, A. Fortunelli, Interface-stabilized phases of metal-on-oxide nanodots, ACS Nano 2 (2008) 1849–1856, http://dx.doi.org/10.1021/nn800315x.
[28] L. Yang, S. Shan, R. Loukrakpam, V. Petkov, Y. Ren, B.N. Wanjala, M.H. Engelhard, J. Luo, J. Yin, Y. Chen, C.J. Zhong, Role of support-nanoalloy interactions in the atomic-scale structural and chemical ordering for tuning catalytic sites, J. Am. Chem. Soc. 134 (2012) 15048–15060, http://dx.doi.org/10.1021/ja3060035.
[29] V. Petkov, Y. Ren, S. Shan, J. Luo, C.-J. Zhong, A distinct atomic structure-catalytic activity relationship in 3–10 nm supported Au particles, Nanoscale 6 (2014) 532–538, http://dx.doi.org/10.1039/c3nr05362h.
[30] B. Hammer, J.K. Nørskov, Electronic factors determining the reactivity of metal surfaces, Surf. Sci. 343 (1995) 211–220, http://dx.doi.org/10.1016/0039-6028(96)80007-0.
[31] G. Kresse, J. Furthmüller, Efficiency of ab-initio total energy calculations for metals and semiconductors using a plane-wave basis set, Comput. Mater. Sci. 6 (1996) 15–50, http://dx.doi.org/10.1016/0927-0256(96)00008-0.
[32] G. Kresse, J. Furthmüller, Efficient iterative schemes for ab initio total-energy calculations using a plane-wave basis set, Phys. Rev. B 54 (1996) 11169–11186, http://dx.doi.org/10.1103/PhysRevB.54.11169.
[33] G. Kresse, J. Hafner, Ab initio molecular-dynamics simulation of the liquid-metalamorphous- semiconductor transition in germanium, Phys. Rev. B 49 (1994) 14251–14269, http://dx.doi.org/10.1103/PhysRevB.49.14251.
[34] G. Kresse, J. Hafner, Ab initio molecular dynamics for liquid metals, Phys. Rev. B 47 (1993) 558–561, http://dx.doi.org/10.1103/PhysRevB.47.558.
[35] J.P. Perdew, K. Burke, M. Ernzerhof, Generalized gradient approximation made simple, Phys. Rev. Lett. 77 (1996) 3865–3868, http://dx.doi.org/10.1103/PhysRevLett.77.3865.
[36] G. Kresse, From ultrasoft pseudopotentials to the projector augmented-wave method, Phys. Rev. B 59 (1999) 1758–1775, http://dx.doi.org/10.1103/PhysRevB.59.1758.
[37] P.E. Blöchl, Projector augmented-wave method, Phys. Rev. B 50 (1994) 17953–17979, http://dx.doi.org/10.1103/PhysRevB.50.17953.
[38] M. Methfessel, A.T. Paxton, High-precision sampling for Brillouin-zone integration in metals, Phys. Rev. B 40 (1989) 3616–3621, http://dx.doi.org/10.1103/PhysRevB.40.3616.
[39] W. Tang, E. Sanville, G. Henkelman, A grid-based Bader analysis algorithm without lattice bias, J. Phys.: Condens. Matter. 21 (2009) 84204, http://dx.doi.org/10.1088/0953-8984/21/8/084204.
[40] A. Ruban, B. Hammer, P. Stoltze, H.L. Skriver, J.K. Nørskov, Surface electronic structure and reactivity of transition and noble metals, J. Mol. Catal. A: Chem. 115 (1997) 421–429, http://dx.doi.org/10.1016/S1381-1169(96)00348-2.
[41] M. Mavrikakis, B. Hammer, J. Nørskov, Effect of Strain on the Reactivity of Metal Surfaces, Phys. Rev. Lett. 81 (1998) 2819–2822, http://dx.doi.org/10.1103/PhysRevLett. 81.2819.
[42] P. Liu, J.K. Nørskov, Ligand and ensemble effects in adsorption on alloy surfaces, Phys. Chem. Chem. Phys. 3 (2001) 3814–3818, http://dx.doi.org/10.1039/b103525h.
[43] Y. Gauthier, M. Schmid, S. Padovani, E. Lundgren, V. Bus, G. Kresse, J. Redinger, P. Varga, Adsorption sites and ligand effect for CO on an alloy surface: a direct view, Phys. Rev. Lett. 87 (2001) 36103, http://dx.doi.org/10.1103/PhysRevLett.87.036103.
[44] J.R. Kitchin, J.K. Nørskov, M.A. Barteau, J.G. Chen, Modification of the surface electronic and chemical properties of Pt(111) by subsurface 3d transition metals, J. Chem. Phys. 120 (2004) 10240–10246, http://dx.doi.org/10.1063/1.1737365.
[45] G. Mpourmpakis, A.N. Andriotis, D.G. Vlachos, Identification of descriptors for the CO interaction with metal Nanoparticles, Nano Lett. 10 (2010) 1041–1045, http://dx.doi.org/10.1021/nl904299c.
[46] Y. Lei, H. Zhao, R.D. Rivas, S. Lee, B. Liu, J. Lu, E. Stach, R.E. Winans, K.W. Chapman, J.P. Greeley, J.T. Miller, P.J. Chupas, J.W. Elam, Adsorbate-induced structural changes in 1–3 nm platinum nanoparticles, J. Am. Chem. Soc. 136 (2014) 9320–9326, http://dx.doi.org/10.1021/ja4126998.
[47] P.C. Jennings, H.a. Aleksandrov, K.M. Neyman, R.L. Johnston, A DFT study of oxygen dissociation on platinum based nanoparticles, Nanoscale 6 (2013) 1153–1165, http://dx.doi.org/10.1039/c3nr04750d.
[48] K.P. McKenna, A.L. Shluger, Shaping the morphology of gold nanoparticles by CO adsorption, J. Phys. Chem. C 111 (2007) 18848–18852, http://dx.doi.org/10.1021/jp710043s.
[49] N. Austin, J.K. Johnson, G. Mpourmpakis, Au_{13}: CO Adsorbs, Nanoparticle Responds, J. Phys. Chem. C 119 (2015) 18196–18202, http://dx.doi.org/10.1021/acs.jpcc.5b03459.
[50] H. Xin, S. Linic, Communications: Exceptions to the d -band model of chemisorption on metal surfaces: The dominant role of repulsion between adsorbate states and metal d -states, J. Chem. Phys. 132 (2010) 221101, http://dx.doi.org/10.1063/1.3437609.